

Electron field emission from ferromagnetic europium sulfide on tungsten

E. Kisker,* G. Baum, A. H. Mahan,† W. Raith, and B. Reihl‡

Fakultät für Physik, Universität Bielefeld, D-4800 Bielefeld, Federal Republic of Germany

(Received 13 March 1978)

The emission process from W-EuS junction field emitters was studied by combination of several experimental methods: measurement of emission current, spin polarization, energy distribution, and energy-selective spin polarization as function of emitter temperature for different annealing conditions. The results show that with critical annealing a stoichiometric crystalline EuS layer can be obtained; the interface of such a layer on tungsten acts as a spin filter below the EuS Curie temperature. With emitters annealed at higher temperatures, evidence for electron trapping and the formation of spin clusters has been obtained.

I. INTRODUCTION

A. Historical remarks

Ferromagnetic semiconductors, in particular the europium chalcogenides, have been of great interest because of their magnetic, optical, and transport properties.¹⁻³ In rare-earth atoms the partially filled $4f$ shell is well shielded by the outer electrons. In europium the seven electrons of the $4f$ shell couple in such a way that the orbital angular momenta add up to zero, whereas the spins result in a total spin of $S = \frac{7}{2}$ for each atom. In the europium-sulfide crystal, which has rock-salt structure, the spins of the Eu^{2+} ions can be coupled by means of an indirect exchange interaction which leads to ferromagnetism below 16.6 K.⁴ The EuS conduction band is split by ferromagnetic exchange, i.e., the bottom of the band is lowered (raised) for electrons with spins parallel (antiparallel) to those of the $4f^7$ electrons. In 1964 this effect was discovered as a red shift of the absorption edge by Busch *et al.*^{5,6} In studies of metal-EuS-metal junctions, Esaki *et al.*⁷ observed a large magnetic effect on the internal field emission which is also caused by this band splitting.

As early as 1930, Fues and Hellmann⁸ proposed field emission from ferromagnetic materials as a method for producing spin-polarized electron beams. The spin polarization of an ensemble of electrons is defined (nonrelativistically) as

$$\vec{P} = \text{Tr} \vec{\sigma} \rho, \quad (1)$$

where $\vec{\sigma}$ is the Pauli spin matrix vector and ρ is the spin state density matrix. Often it suffices to define the degree of polarization as the difference of the number of electrons having their spins parallel and antiparallel to some axis of quantization, divided by the sum of the numbers. The average polarization of *all* the electrons in a ferromagnetic material is rather low, e.g., $P_{av} = 0.08$ for the electrons in iron. In field emission from a ferromagnetic metal, however, the polarization of the

emitted electrons is determined by the differences in the density of the two spin states near the Fermi edge, which can be considerably higher than the average.⁹ Since the early polarization experiments with metals yielded rather low polarizations,¹⁰⁻¹⁶ these studies were extended to ferromagnetic semiconductors. A very high polarization of electrons from W-EuS field emitters was first observed by N. Müller *et al.* in 1972.¹⁸ Our own investigations of the same emitter system have proved that the emission process involves electron tunneling from the Fermi level of tungsten into the split EuS conduction band, where the internal barrier at the W-EuS interface is of different heights for the two electron-spin states and, therefore, acts as a spin filter.¹⁹

B. Interest in polarized electron sources

A source of spin polarized electrons can be utilized in scattering experiments to investigate spin-dependent electron interactions. Great scientific interest in such experiments exists in atomic, high-energy, and solid-state physics. Several sources of polarized electrons are available,^{20,21} and the physicist, planning an experiment with polarized electron beams, has to select the source which best suits his needs. For low-energy experiments, the W-EuS field-emission source appears to be particularly useful since it is almost a point source representing an emitter of extremely high brightness. A comparison with other sources, also suitable for experiments with low-energy electrons, will be given in Sec. V.

C. Goals of this investigation

This work was originally stimulated by our interest in polarized electron sources for atomic physics scattering experiments. However, it soon became clear that the processes involved in electron emission from W-EuS emitters are very complex and not well understood. Therefore, we

did not want to limit the studies to finding the optimum operating conditions of a field-emission polarized electron source but rather to aim for an understanding of the physics of W-EuS emitters. These studies led to the discovery of several phenomena which are new in the area of electron field emission and which provide information on structure and ferromagnetism of europium sulfide. We are now able to interpret our results in a consistent way, although some questions still remain and demand further experimental investigations. Preliminary results have already been communicated.^{19,22-24}

II. EXPERIMENTAL ARRANGEMENT

A. Layout, vacuum, and high voltage

A side view of the apparatus is shown in Fig. 1. The electron beam goes horizontally from left to right. The field-emission chamber on the left side contains the electron source. It is a bakeable ultrahigh-vacuum (UHV) system in which a pressure in the range 10^{-10} – 10^{-11} Torr is maintained during operation. There are two pumps connected to the chamber, a small turbomolecular pump (pumping speed about 40 liter/sec at the chamber) and a titanium getter pump (1200 liter/sec). The turbomolecular pump alone produces a vacuum of 2×10^{-9} Torr after 250 °C bakeout. The very low pressure is obtained in about 24 h after titanium evaporation. The turbomolecular

pump remains connected to the system for inactive gas pumping. The next chamber is a differential pumping chamber (40×10^{-9} Torr) which is necessary for reducing the gas stream from the Wien filter chamber into the source chamber. The Wien filter and Mott-scattering chambers (10^{-6} – 10^{-7} Torr) are both pumped by a second turbomolecular pump.

The cold finger to which the emitter is mounted is attached to the field-emission chamber via an electrically insulating glass-to-metal transition piece. This permits the cold finger and the attached cooling system (helium Dewar and transfer line) to be floated at a potential of -2 kV with respect to ground. The walls of the first three chambers are grounded, and the Mott-scattering chamber, connected to the end of the accelerator, is kept at +100 kV.

B. Tip mounting

The cold finger permitted quick variation of the tip temperature in the range between 40 and 9 K, the interesting region above and below the Curie point of EuS. It was cooled dynamically, as described by Reed and Graham.²⁵ The temperature is varied by adjusting the two-phase (part liquid, part gaseous) helium flow. The latest version of our system is shown in Fig. 2. It has the advantage of requiring only one insulated electrical feedthrough, thereby reducing space requirements

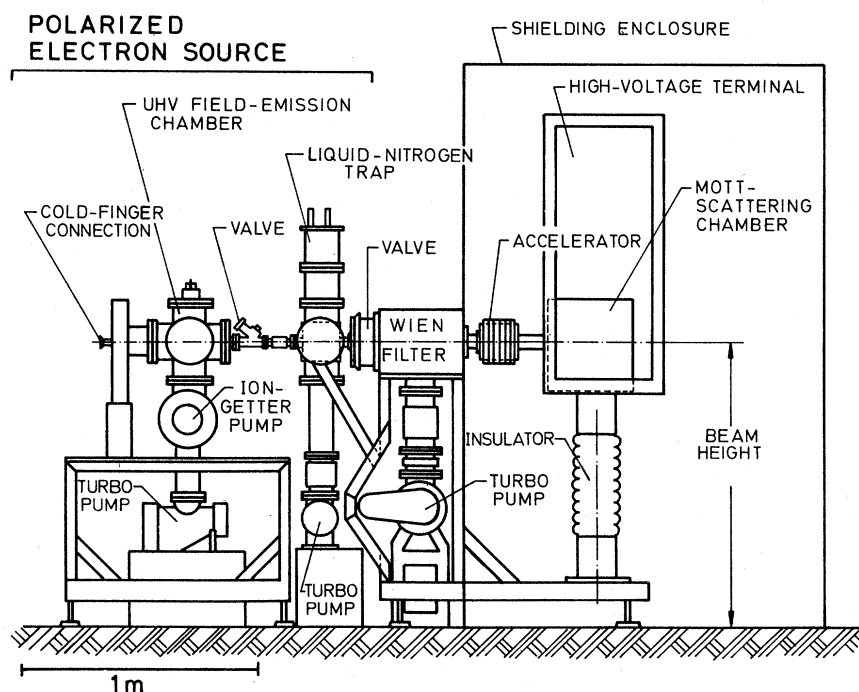


FIG. 1. Side view of apparatus.

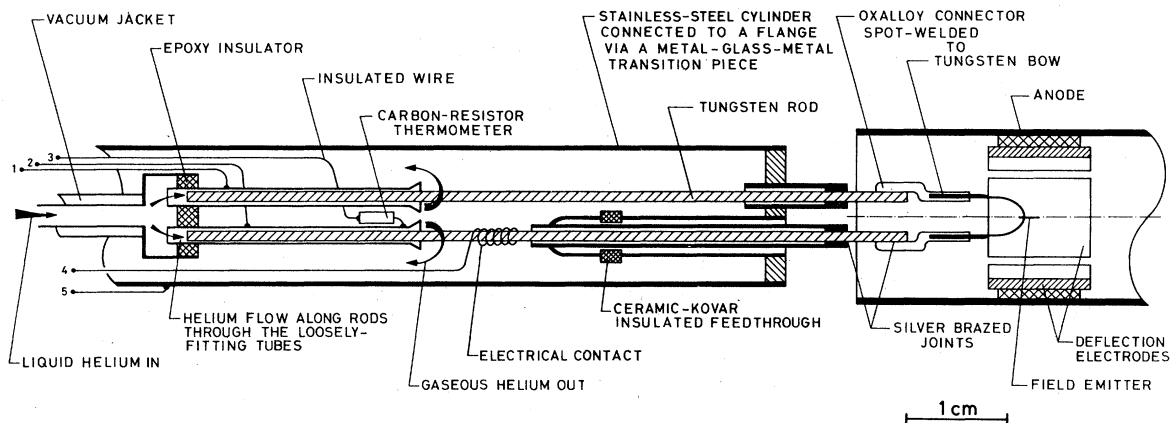


FIG. 2. Cross section of cold finger with emitter-support structure and anode region. Electrical connections: (1) + (2)—heating current through tungsten bow; (2) + (3)—carbon thermometer; (4) + (5)—potential drop across bow; (5)—emitter potential of several kilovolts with respect to ground. The liquid-helium inlet pipe together with the tubes, carbon thermometer and wire nos. 1-3 form a plug which is inserted from the left.

and the possibility of vacuum leaks. During operation the temperature is monitored by the carbon-resistor thermometer located near the helium flow tubes. The temperature is electronically regulated by adjusting the flow valve such that the carbon resistance is kept at a preselected value.

C. Europium-sulfide deposition

We used commercial tungsten tips with the $\langle 110 \rangle$, $\langle 111 \rangle$, or $\langle 112 \rangle$ direction parallel to the tip axis.²⁶ The EuS was evaporated onto the tungsten tip in the field-emission chamber from an oven of 5-mm diameter and 6.5-mm height, moved sideways onto the beam axis at a distance of 7 cm from the tip. The oven, which was surrounded by a heat shield, was heated by bombardment with a 180-mA current of 500-eV electrons, yielding an oven temperature of about 2300 K. One oven filling of 0.2-g EuS (see Ref. 27) lasted for

about 20 depositions. During all depositions the electron-beam current for heating the oven was the same as that used in a separate measurement of the EuS deposition rate. The rate was determined by depositing EuS onto the surface of a quartz oscillator and observing the change of its eigenfrequency due to the increase of mass.^{28,29} It was found that the rate of EuS deposition onto the tungsten tip was 400 Å thickness per minute of evaporation. This is consistent with a calculation using the vapor pressures of Eu and S as given by Smoes et al.³⁰ and assuming that EuS decomposes in the oven and recombines during annealing of the deposited layer.

D. Electron optics

The electron-optical elements are shown schematically in Fig. 3. The emitter is surrounded by a solenoid which produces a longitudinal magnetic field at the tip. This magnetic field has two pur-

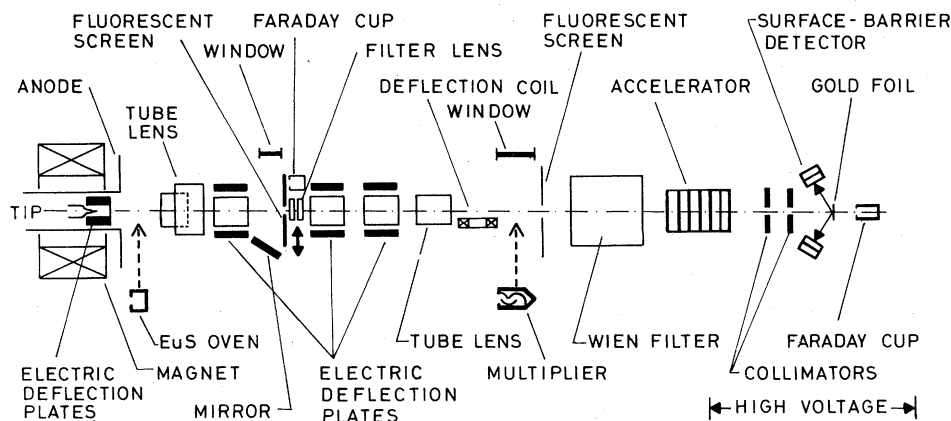


FIG. 3. Schematic drawing of experimental arrangement (not to scale).

poses: firstly, it combines with the radial electric field at the tip in order to focus the field-emission image onto the fluorescent screen; secondly, it affects the magnetization of the EuS layer and enables the emission process to be studied in high magnetic fields. The tube lens in front of the fluorescent screen can be used to change the magnification of the field-emission pattern; its main function, however, is to shield the beam against electrostatic stray fields. The tube lens downstream from the probe hole focuses and transports the beam into the differential pumping chamber and the Wien-filter chamber.

Most studies were made in a weak longitudinal field of 25–250 G which was produced by the solenoid. Typically, a first image crossover occurs at 25 G. In a weak longitudinal magnetic field, or in zero field, the EuS layer is spontaneously magnetized in a direction tangential to the surface and transverse to the tip axis as is shown by our polarization measurements. With no applied transverse magnetic field the actual direction of the magnetization is determined by spurious stray fields. When the tip temperature temporarily goes above the Curie point—as happens when a gas bubble flows through the cooling system—the transverse magnetization and the polarization may reverse its direction. In order to insure a definite direction of magnetization two pairs of coils, producing a horizontal and vertical transverse field, respectively, were mounted inside the copper-coil magnet. For the high-field studies a water-cooled iron-clad coil was used, which yielded a field of up to 5.2 kG at the tip, falling off toward the anode more rapidly than the weak field produced by the solenoid. With this magnet the first focus is obtained at about 200 G.

Various electric and magnetic beam deflection devices are placed along the beam line for achieving optimum beam transport. In order to eliminate effects of the earth's magnetic field on the long electron beam path, the beam axis is oriented in the north-south direction, and the vertical component of the earth's field is compensated with a horizontal coil.

E. Faraday cup and filter lens

The design of the Faraday cup which was used for the retarding field energy-distribution measurements is shown in Fig. 4. In order to obtain a uniform contact potential the cup was gold coated on the inside and on the front. The cone on the back surface is intended for reducing the emission of secondary electrons out of the cup. By means of a linear motion feedthrough the cup can be moved in and out of the electron beam.

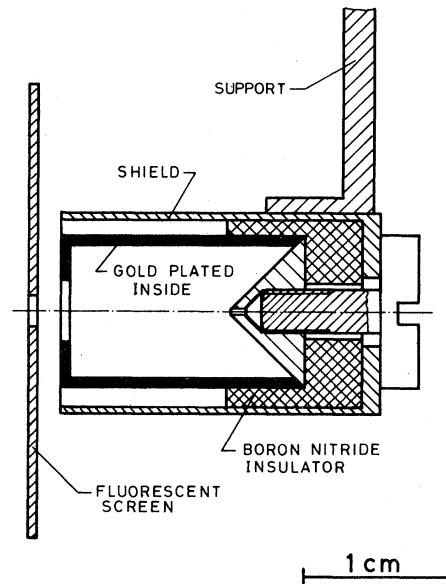


FIG. 4. Cross section of Faraday cup.

A filter lens is used in measuring the spin polarization of electrons having an energy exceeding a selected threshold energy E_{th} . Its design is shown in Fig. 5. The filter lens is mounted on the same support bar as the Faraday cup which permits movement transverse to the beam line.

Figure 6 shows the electronic instrumentation

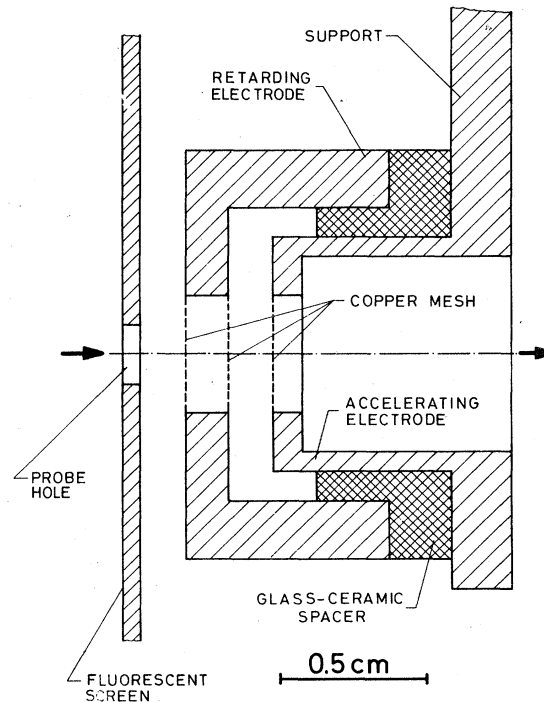


FIG. 5. Cross section of filter lens.

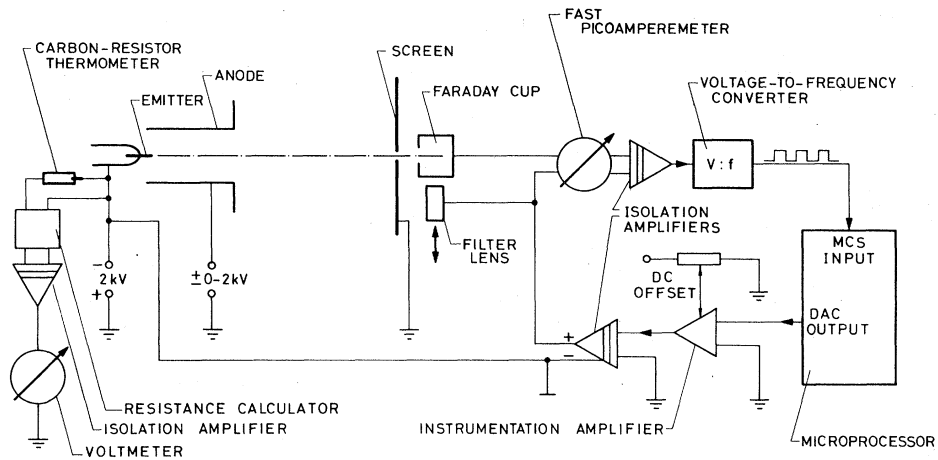


FIG. 6. Electronics for measurements of the cold-finger temperature (left-hand side) and of the electron energy distributions (right-hand side). MCS: multi-channel scaling, DAC: digital-analog converter.

for the energy distribution measurements together with that for monitoring the cold-finger temperature. The Faraday-cup current is measured by means of a fast electrometer operated in the feedback mode in order to minimize the voltage drop across its input resistance. The retarding voltage applied between tip and Faraday cup is increased in small steps. This staircase voltage is controlled by a microprocessor which is also programmed to perform as a multichannel analyzer (MCA) in the multiscaling mode.³¹ The current signal is digitized by a voltage-to-frequency converter and added to the memory of the corresponding channel. The current as a function of retarding voltage is measured over several sweeps. From these integral energy distributions the differential distributions are obtained by differentiation, also done by the microprocessor. The differential energy distribution is displayed on line and also put on tape.

F. Wien filter and Mott detector

The electron polarization is determined by Mott scattering from a gold target at an electron energy of 100 keV. If the beam is transversely polarized, the intensity distribution of the back-scattered electrons is anisotropic and the polarization component perpendicular to the scattering plane can be determined from the counting rates of two detectors located at azimuthal angles $\phi = 0^\circ$ and 180° (which are both at a polar angle of $\Theta = 120^\circ$).

Actually, we used *four* surface-barrier detectors³² at azimuthal angles of 0° , 90° , 180° , and 270° for measuring both transverse components of the polarization simultaneously. In addition, the longitudinal component of the polarization can be measured by converting it into a transverse

one. This conversion is achieved with a Wien filter, consisting of crossed static electric and magnetic fields, both of which are perpendicular to the beam direction. The electric field is adjusted to a value such that the electric force compensates the Lorentz force, and the electron beam goes straight through the Wien filter. The spin, however, precesses around the magnetic field direction and the magnetic field is set such that the total precession angle is 90° .

The design of the Wien filter is shown in Fig. 7. Besides turning the polarization vector, the Wien filter also has electron-optical properties. In the plane perpendicular to the magnetic field, the filter acts like a positive lens. We adapted a Wien-filter design which also provides focusing in the plane perpendicular to the electric field by using curved capacitor plates,³³ thus achieving a higher filter transmittance.

The design of the Mott-scattering apparatus is very similar to one used previously.³⁴ Details of the arrangement are shown in Fig. 8. The accelerator consists of six electrodes connected to a voltage divider. In the Mott chamber, a wheel carries four different scattering foils. The gold foils were produced by evaporating gold onto a Formvar³⁵ carrier foil. By employing foils of different thicknesses the scattering asymmetry can be extrapolated to zero foil thickness, a procedure which eliminates the influence of multiple scattering within the gold foil. This procedure requires only knowledge of the relative foil thickness, which can be obtained from comparing the count rates of electrons scattered from the different foils at constant primary beam intensity.

The detector asymmetries were measured with a thick aluminum scattering foil for which the Mott-scattering asymmetry is negligibly small. Several collimators (C_1 to C_6 in Fig. 8) serve to

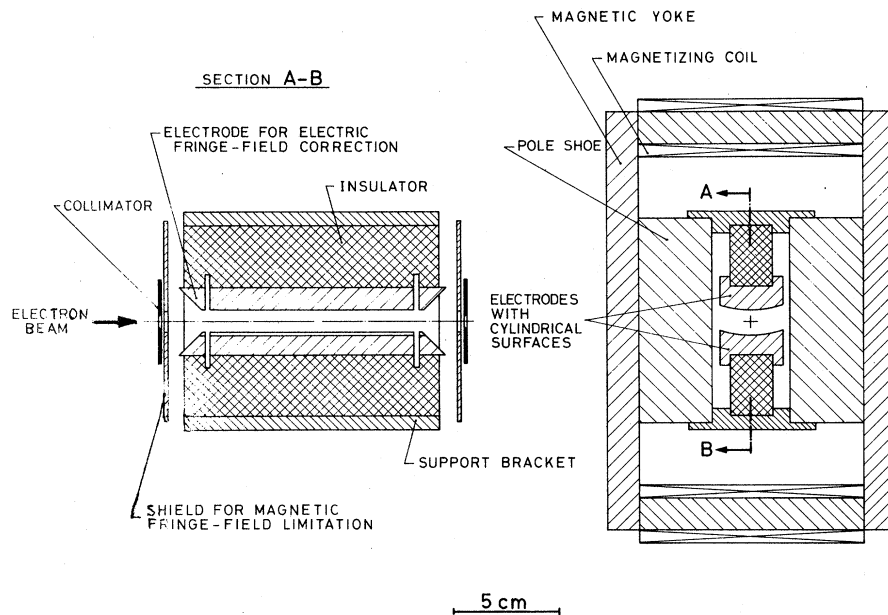


FIG. 7. Cross sections through Wien filter.

suppress wall-scattered electrons. In addition the Mott chamber has a large volume, the walls are of low- Z material to favor energy losses, and surface-barrier detectors are used which permit electronic pulse-height discrimination.

The data acquisition system is shown schematically in Fig. 9. The pulses from the surface-barrier detectors are amplified and fed to light-emitting diodes. The light pulses are transmitted across the 100-kV potential difference to photodiodes at ground potential. From there, the pulses are amplified again, and transferred to a multichannel analyzer for pulse-height analysis. Thus, for any polarization measurement, the

pulse-height distributions of the four detectors are measured and the count rates are obtained by integrating over the elastic peak. This method has the advantage that the pulse-height distributions and accompanying thresholds are continuously monitored and, therefore, changes in the distributions caused by excessively high count rates or temperature effects in the electronic arrangement are immediately recognized.

In the energy selective measurements of the polarization four single-channel analyzers are used; their output pulses are fed to the micro-processor which in those measurements is utilized as a four-input multichannel scaler.

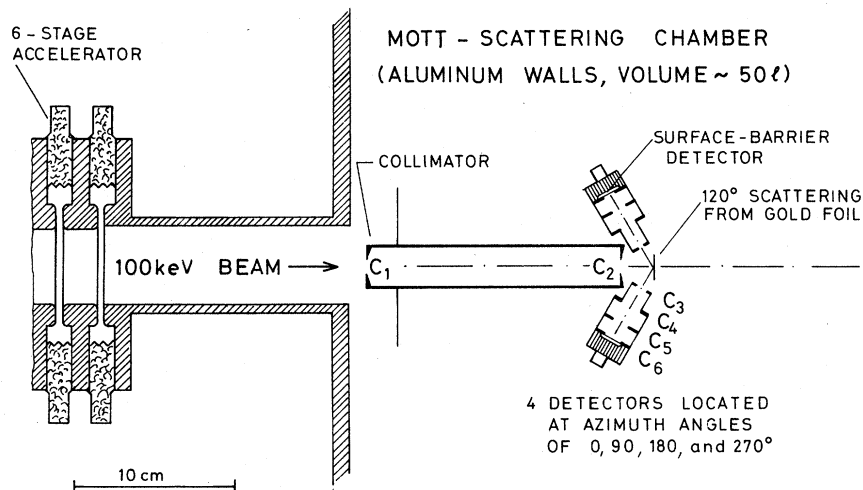


FIG. 8. Some details of the Mott-scattering polarization analyzer. The aluminum electrodes and ceramic insulators of the accelerator were glued together by means of vinyl acetate dissolved in toluene.

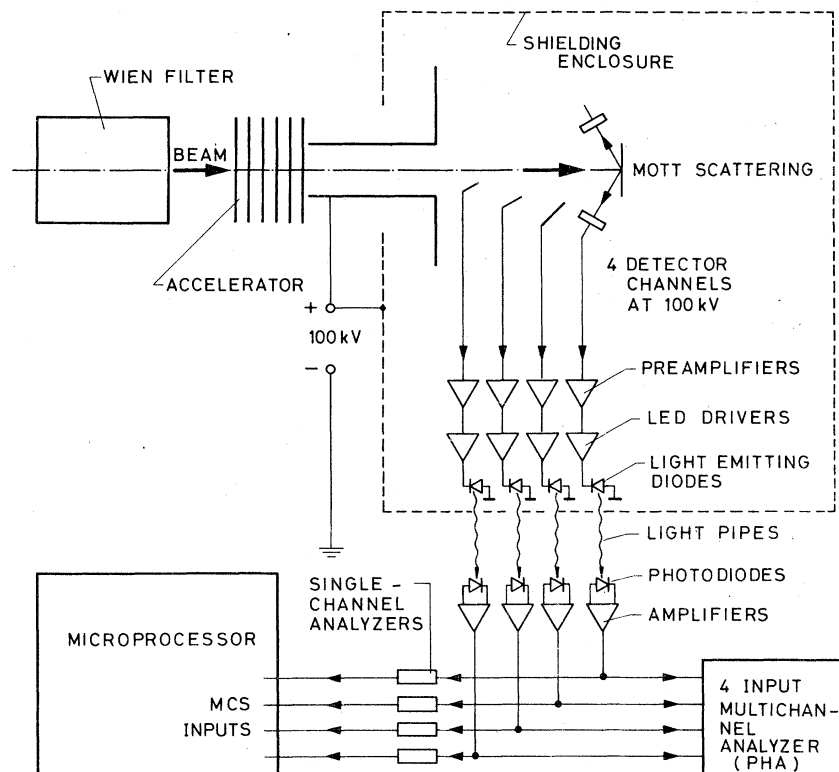


FIG. 9. Data acquisition system for Mott scattering (PHA: pulse-height analyzer).

III. EXPERIMENTAL PROCEDURES

A. Tip preparation

Prior to inserting the cold finger (Fig. 2) into the apparatus, the tip was adjusted mechanically by bending the tip support filament so that the tip was centered on the axis of the cold finger to within 1 mm. After bakeout of the apparatus, the tip was flashed and thereby cleaned and the tungsten field-emission pattern observed on the fluorescent screen. With the help of a mechanical adjustment device, the cold finger was moved laterally until the field-emission pattern rotated around the central spot when the magnetic field was varied. This insures that the tip axis coincides with the axis of the magnetic field.

During EuS deposition, the tip is electrically grounded and at room temperature. The pressure in the field-emission chamber goes up into the 10^{-8} -Torr range when the EuS oven is heated. The annealing process is started after a pressure of about 10^{-10} Torr has been reached again, and the field-emission studies are begun only after annealing and subsequent cooling. (If emission current is drawn from an uncooled and not sufficiently annealed emitter, this emitter is most likely destroyed by a sudden, drastic current increase.)

Annealing of the EuS layer is facilitated by direct heating of the tungsten bow. The tip temperature during annealing T_A is determined from the resistance of the tungsten bow, which is obtained from the ratio of the voltage drop across the bow to the heating current.³⁶ Since the current leads connected to the tip bow must be thin in order to reduce heat conduction to the tip, annealing was done only when the emitter had been cooled below 20 K. This reduced the electric resistance of the copper leads and of the tungsten pins so that heating occurs practically only at the front part of the tungsten bow (which is etched thin in the vicinity of the tip-wire welding point). In this way, the voltage drop, measured across the leads (Nos. 4 and 5 of Fig. 2), is nearly equal to the voltage drop across the heated part of the tungsten bow.

In most of the studies described here, an analog circuit was used for regulating the heating current such that a preselected annealing temperature T_A is maintained for a few seconds. This method of temperature regulation has been replaced by a digital one, employing the microprocessor. The T_A determination based on tungsten resistance was checked at higher temperatures by a comparison with pyrometric observation.

After annealing the tip is cooled to 10 K before the extraction voltage is applied. Typically the

extraction voltage was increased slowly until the total emission current from the tip amounted to some 10^{-9} A; if this current was not obtained below a certain voltage, the tip was reannealed at a slightly higher temperature and the process repeated, if necessary.

B. Measurement of tip temperature during operation

The carbon-resistor thermometer built into the cold finger (cf. Fig. 2) was purchased with a certified calibration.³⁷ During operation it measured the temperature at some distance from the tip. In a separate test, a second carbon-resistor thermometer was glued with high-thermal-conductivity epoxy to one of the two tungsten support rods (Fig. 2) on the vacuum side of the cold finger, and in this way the temperature difference between the two locations was determined. The absolute uncertainty of the tip-temperature determination is estimated as ± 1 K.

C. Observation of field-emission pattern

A weak longitudinal magnetic field was employed for producing a small image of the field-emission pattern at the first fluorescent screen (cf. Fig. 3 and Sec. IID). Lack of space prevented observation of a large angle field-emission pattern which would be obtained in a radial electric field in the absence of a longitudinal magnetic field.

D. Measurement of current-voltage characteristics (Fowler-Nordheim plots) and of the current-temperature dependence

Current-voltage characteristics were obtained by imaging the pattern onto the fluorescent screen and measuring the screen current, which was usually about 90% of the total emission current. The latter could not be measured with the desired accuracy because of leakage to ground. If the pattern expanded too much when the emission voltage was changed, the pattern was demagnified again by adjusting the magnetic field. This method yielded straight Fowler-Nordheim (FN) plots for the clean tungsten emitter over two orders of magnitude of current change.

Measuring FN plots for W-EuS was more difficult than for clean tungsten because of the very strong dependence of emission current upon tip temperature.¹⁹ Since this temperature varied by about ± 1 K periodically due to oscillations in the cooling system, the tip temperature and, in turn, the emission current oscillated also. The mean value of the oscillations was used. An ideal measurement would consist of a FN plot for that part of the W-EuS pattern which is selected by the

probe hole for subsequent polarization and/or energy distribution analysis. Unfortunately, this was impossible because of the movement of the image when the extraction voltage was changed; in particular, the magnetic field could not be re-adjusted with sufficient accuracy for obtaining constant image conditions.

The dependence of emission current upon tip temperature, however, could be measured with this probe-hole technique because here the electron optical conditions remain unchanged. Therefore, using the Faraday cup behind the probe hole as an electron collector, the $I(T)$ curves could be measured conveniently by connecting the Y-axis of an X-Y recorder to the electrometer output and the X axis to a signal which was proportional to the value of the carbon-resistor thermometer (see Fig. 6).

When the polarization was measured, the mean count rate of the Mott detectors was taken as a measure of the current.

E. Measurement of electron-energy distributions

Before the energy distribution of an EuS coated tip was measured, the clean-tungsten energy distribution was taken in order to check the experimental resolution of the retarding-field analyzer. The energy resolution was found to be 150 meV, independent of the magnetic field strength up to about 1 kG. The voltage corresponding to the Fermi level of tungsten was taken as the zero value of the energy scale. It depends only slightly on the beam adjustment (it shifted not more than 0.2 V when the outermost parts of the pattern were moved onto the probe hole by electric or magnetic deflection). With our experimental arrangement, the *total* energy of the electrons is measured; this can be concluded from the literature on such retarding-field analyzers.^{38,39}

F. Measurement of the electron-spin polarization

The two transverse components of the polarization vector are measured simultaneously by two orthogonal sets of detector pairs. The beam intensity was adjusted to yield count rates of 1000 to 20,000 counts per second. In order to determine the longitudinal component of the polarization, a separate measurement is made using the Wien filter for polarization conversion. In each polarization measurement, the count-rate ratio of a detector pair N/N' is corrected for the instrumental asymmetry effects of the apparatus; the correction is determined by scattering from an aluminum foil, keeping the same scattering geometry. From the corrected ratio

$$R = (N/N')_{A0} / (N/N')_{A1} \quad (2)$$

follows the measured asymmetry

$$\Delta = (1 - R) / (1 + R). \quad (3)$$

The asymmetry has to be corrected for the influence of the foil thickness by extrapolation to zero thickness according to

$$\Delta_0 = \Delta(1 + a), \quad (4)$$

where a is a constant which is proportional to the thickness of the foil employed. For the foils used the constant a ranged from 0.20 to 0.45. For a given detector pair the extrapolated asymmetry is related to the corresponding component of the polarization vector by

$$P_i = \Delta_{0,i} / S, \quad (5)$$

where S is the value of the "Sherman function," that is, the analyzing power of the Mott scattering.³⁴ Here, $S = 0.40$ for $E = 100$ keV and $\theta = 120^\circ$.

For W-EuS emitters prepared in a certain way (cf. Sec. IVD) the electron-energy distribution consists of two peaks which are separated by more than 1 eV. In order to measure polarization with energy selection, a filter lens was employed which could be moved behind the probe hole. This lens only transmitted electrons with "normal energy" (that is, $\frac{1}{2}mv_z^2$, where z is the coordinate normal to mesh of filter lens) greater than the threshold energy, the latter being proportional to the potential of the middle electrode. This potential was increased stepwise by the microprocessor, and for each step the count rates of the four Mott detectors were stored in the memory of the microprocessor board. These runs were repeated and accumulated several times in order to obtain a reasonable number of counts even in the high-energy region of the energy distributions where the count rates are small. A measurement with the aluminum foil was performed to assure that the experimental asymmetry did not depend on the potential of the middle electrode.

IV. RESULTS AND INTERPRETATIONS

A. Dependence of field-emission current and spin polarization on tip temperature

The most striking property of the W-EuS emitters is the strong dependence of emission current on tip temperature below the Curie point, which had not been observed before in any field emission experiment. This occurs with emitters annealed at temperatures of about 800 to 1000 K for some seconds (or at 600 K for 1 h). With these annealing conditions the total emission current increases by several orders of magnitude upon cooling

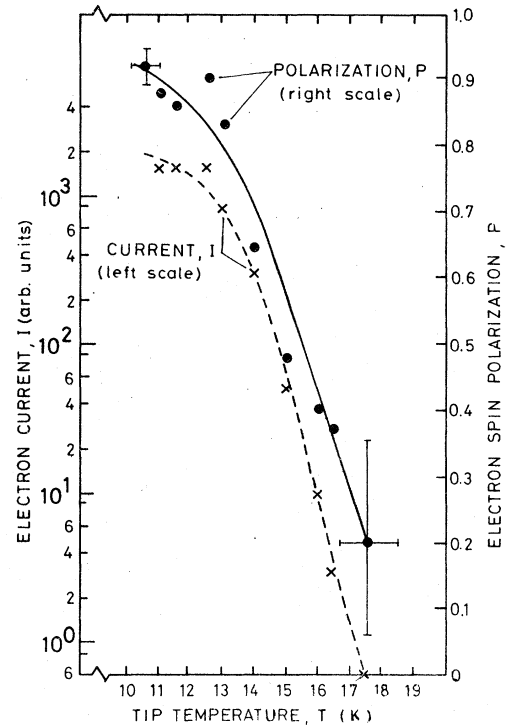


FIG. 10. Electron current going through probe hole and electron-spin polarization vs tip temperature. The solid curve gives values of $M_I = P(4f^I)$ calculated from Eq. (8) by using the $I(T)$ measurements (dashed curve).

from 17 to 9 K, as shown in Fig. 10. This pronounced current-temperature dependence is explained with the band model shown in Fig. 11. Since EuS is an insulator, the EuS energy bands are tilted when an external electric field is applied. If field strength and film thickness are sufficiently large, the bottom of the EuS conduction band is lowered below the tungsten Fermi level, and electrons can tunnel from tungsten into the EuS conduction band and from there into vacuum. The dependence of emission current upon tip temperature is explained by the lowering of the conduction-band bottom (for electrons in one spin state) due to the ferromagnetic exchange splitting, by which the tunneling probability into the EuS is greatly enhanced. Conversely, the height of the external barrier with respect to the lower edge of the conduction band increases. This, however, is assumed to have only a minor effect because the relative change is much smaller.

The tunnel-current density into the EuS is given by

$$j(T) = [AF_i^2 / \phi_i(T)] \exp[-b\phi_i(T)^{3/2} / F_i], \quad (6)$$

where A and b are constants, F_i (F_e) is the internal (external) electron field strength ($F_i = F_e / \epsilon$),

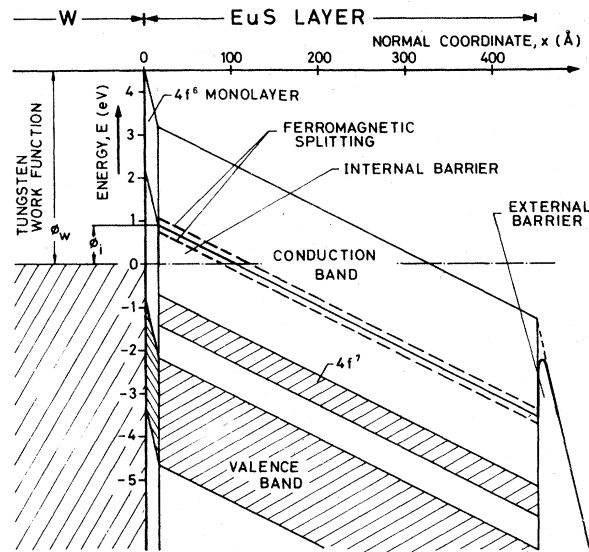


FIG. 11. Band model for the W-EuS field emitter. In this drawing a EuS-layer thickness of 450 Å and an external field strength of 10^7 V/cm were assumed.

ϵ the dielectric constant, and ϕ_i the height of the internal barrier. Thus the logarithm of the emission current I is related to ϕ_i by

$$\frac{\ln I(T) - \ln I(T_C)}{\ln I(0) - \ln I(T_C)} = \frac{\phi_i(T_C)^{3/2} - \phi_i(T)^{3/2}}{\phi_i(T_C)^{3/2} - \phi_i(0)^{3/2}} \approx \frac{\phi_i(T_C) - \phi_i(T)}{\phi_i(T_C) - \phi_i(0)} \quad (7)$$

where $I(0)$ and $I(T_C)$ are the emission currents at $T=0$ and $T=T_C$, respectively, and $\phi_i(0)$ and $\phi_i(T_C)$ the corresponding heights of the internal barrier. Since $\phi_i(T)$ varies within a limited range, the linear approximation for the right-hand side of Eq. (7) can be used with good accuracy. (The current of electrons in the other spin state, for which the bottom of the EuS conduction band is raised, can be neglected completely.)

In studies of In-EuS-In tunnel junctions Thompson *et al.*⁴⁰ found that the relative change in internal barrier height is proportional to the relative magnetization, $M(T)/M(0)$.⁴¹ Following their evaluation procedure, we use the logarithm of the current, scaled and normalized in accordance with Eq. (7) as a measure of the magnetization. For the purpose of comparing different magnetization measurements later, we define the relative magnetization inferred from the current data as

$$M_I(T) = \frac{\ln I(T) - \ln I(T_C)}{\ln I(0) - \ln I(T_C)} \quad (8)$$

The relative magnetization is equal in magnitude

to the spin polarization of the ferromagnetically ordered $4f^7$ electrons, $P(4f^7)$. From the electron emission current shown in Fig. 10 (left scale) we computed the function $M_I(T)$ according to Eq. (8) and plotted it as a solid curve (right scale). The curve $M_I = P(4f^7)$ agrees well with the data points for the polarization of the emitted electrons. It must be noted, however, that near T_C , the $P(T)$ values could not be determined very accurately because of temperature oscillations of the cooling system.

An internal barrier which is significantly different for the two electron spin states should act like a perfect spin filter, yielding a polarization of unity at all temperatures below T_C . However, all measured values of $P(T)$ lie below unity (cf. Fig. 10). The fact that $P \approx P(4f^7)$ can be explained by assuming that the internal barrier is a perfect spin filter and that the electron polarization is subsequently reduced by spin-exchange with the $4f^7$ electrons; this spin exchange appears to be likely especially when the electrons lose energy on their way through the EuS and, thus, are energetically near the bottom of the conduction band. In connection with work on photoelectron emission from EuS a high spin-exchange cross section has been estimated.⁴² On the other hand, the internal barrier might not be a perfect spin filter if that portion of the conduction band, which is lowered by the ferromagnetic band splitting, contains a mixture of spin states.^{43,44}

Emitters which have been annealed higher than 1100 K do not display the dramatic current increase upon cooling; instead, within a narrow range of annealing temperatures they sometimes exhibit a current decrease upon cooling as shown in Fig. 12. The current decrease cannot be explained by a change in internal barrier height at the W-EuS interface. The behavior is most likely caused by a bulk effect inside the EuS-layer. Tentatively we assume that those emitters are not ferromagnetic anymore (otherwise they would exhibit a current increase on cooling) and, therefore, the internal barrier is not split and not a spin filter. Instead, we suppose that those emitters have spin clusters around electron traps (cf. Sec. IV. E) which order among each other ferromagnetically below the temperature at which the current change occurs. (Similar ordered clusters in EuTe were described by Vitins and Wachter.⁴⁵) The resulting influence on the energy levels is much weaker than that caused by the normal ferromagnetic ordering of EuS; it does not cause a substantial splitting of the internal barrier but lowers each trap level. These levels lie somewhat below the conduction band. Thus, at temperatures below the current change a trap-hopping electron must tunnel through

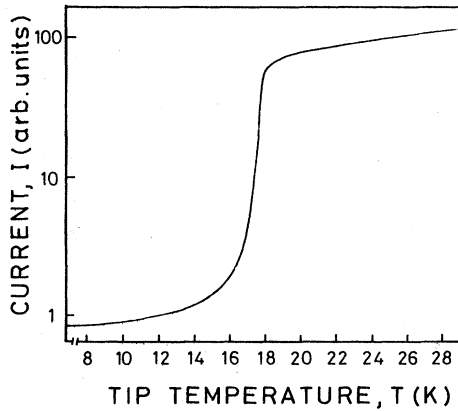


FIG. 12. Current-temperature dependence for an emitter annealed at a temperature above 1100 K. In contrast to the behavior shown in Fig. 12, this current decreases upon cooling.

some barrier each time it penetrates from a trap into the inclined conduction band. At higher temperatures, this tunneling becomes easier because the barrier is reduced and, therefore, the current increases.

The interpretation above invokes spin clusters which order among each other *ferromagnetically* at low temperatures. This phenomenon is different from that discussed later in Sec. IV.H in order to explain the large polarization observed in high external magnetic fields near or above the Curie point; there the clusters are assumed to order *paramagnetically* in the external magnetic field.

B. Influence of annealing on the extraction voltage

It is rather difficult to extract from the available body of data, obtained with emitters of different tip size and EuS-layer thickness, the influence of the annealing temperature upon the emitter characteristics. The extraction voltage V , at which a certain emission current (10^{-9} A) is obtained, was found to depend on both R and d ; next, the electric field strength at the EuS-vacuum boundary was tried as quantity for the intended data evaluation. This field strength is given by

$$F_{\text{EuS}} = V/k(R+d), \quad (9)$$

where k is geometric form factor.⁴⁶ Because the factor k is not known, one can eliminate k by using the field strength F_w at which the same emission current is obtained *with the same, but clean tungsten emitter* before EuS deposition. This leads to the following ratio of field strengths and extraction voltages, respectively,

$$F_{\text{EuS}}/F_w = V_{\text{EuS}}/V_w(1+d/R). \quad (10)$$

The right-hand side of Eq. (10) contains only measurable quantities and, therefore, we use this expression to define the "normalized extraction voltage"

$$V_N = V_{\text{EuS}}/V_w(1+d/R), \quad (11)$$

which we finally used for the data evaluation. The tip radius R contained in Eq. (11) was computed in a rough approximation by assuming a proportionality between R and V_w for all tips used regardless of their shape, $R(\text{\AA}) \sim 0.7V_w(\text{Volt})$.⁴⁷ For d we used the EuS-layer thickness before annealing as determined from the rate of EuS deposition; the thickness after annealing would be more appropriate but this is not known.

Phenomenologically, this method of comparing emitter properties is justified by its success in displaying a great variety of data in the form of one V_N vs T_A curve, as shown in Fig. 13.⁴⁸ The most noticeable features are the sharp maximum of $V_N(T_A)$ at $T_A = 840$ K and the minimum at $T_A = 920$ K, which is followed by a steep rise.

As a tentative interpretation of the function V_N vs T_A we propose the following: The increase of V_N going from $T_A \sim 700$ to 840 K is a consequence of an increase in crystal order; similarly, ordered EuS films were found to have a higher photothreshold than disordered films.⁴⁹ The decrease of V_N going from $T_A \sim 840$ K to 920 K is related to a decrease of the internal barrier at the W-EuS interface which gradually becomes epitaxial and develops a dipole layer reducing the barrier height. As discussed in Sec. IV.D sulfur ions penetrate below the plane of the uppermost tungsten-atom layer into lattice sites such that each S ion can contact with an overlying Eu ion. The rise of V_N going from $T_A \sim 920$ K to about 1000 K results from the decreasing conduction-band splitting caused by the introduction of impurities (stoichiometric imperfections such as S vacancies) into the EuS crystal itself; this phenomenon is also responsible for the accompanying increase in Curie temperature from 16.6 to 23 K.

C. Dependence of emission current on extraction voltage

The dependence of emission current on extraction voltage can be used to calculate the emitter work function. Conveniently, $\ln(I/V^2)$ is plotted versus $1/V$ (Fowler-Nordheim plot), and from the slope m of this curve the work function is obtained.⁴⁶ This method is only meaningful if the curve is a straight line which is approximately the case for our W-EuS emitters having the pronounced dependence of emission current on temperature as shown in Fig. 10. Such Fowler-Nordheim plots with different slopes for two temperatures are

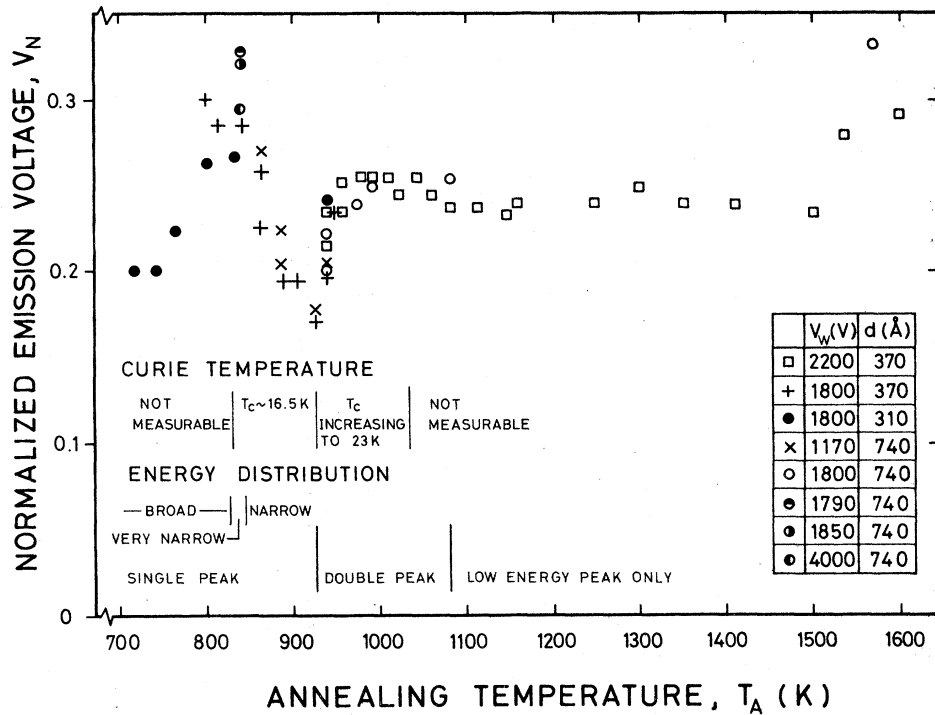


FIG. 13. Phenomenological survey of W-EuS emitters. The normalized emission voltage is given by $V_N = (V/V_W) R/(R+d)$, where V and V_W are the voltages at which an emission current of 10^{-8} A is drawn (at 10K) from the W-EuS emitter and the uncoated W tip, respectively; R is the W tip radius and d is the EuS-layer thickness before annealing. Annealing at the temperature T_A was done for at least 0.5 sec. It was found that the observable effects illustrated in this diagram are not appreciably changed by prolonged annealing at the same temperature, except for the critical annealing at about 840 K. Previous annealing at lower temperatures does not affect the behavior after annealing at a higher temperature. Since the absolute determination of the tip temperature during annealing is rather difficult, the absolute values of T_A could be off by as much as 150° (probably, the true values of T_A lie somewhat lower).

shown in Fig. 14. From the slope m_{EuS} of the FN plot, the work function can be calculated by means of

$$\phi_{EuS} = (-m_{EuS}/b)^{2/3}, \quad (12)$$

where b is the same constant as in Eq. (6). Our $I(T)$ measurements have shown that the current is dominated by the internal barrier ϕ_i , whereas ϕ_{EuS} has no physical meaning. Therefore, we call ϕ_{EuS} an "apparent work function." The measured slope m_{EuS} can be related to ϕ_i by assuming that the field emission process occurs at the W-EuS boundary without any additional tunneling at the EuS-vacuum boundary; it follows that

$$m_{EuS} = -b\epsilon[R/(R+d)]\phi_i^{3/2}, \quad (13)$$

where ϵ is the static dielectric constant of EuS. The proportionality constant b can be eliminated by measuring the slope m_W of a clean W emitter having the same radius R . This yields

$$\phi_i = \left(\frac{m_{EuS}}{m_W} \frac{1}{\epsilon} \frac{R+d}{R} \right)^{2/3} \phi_W, \quad (14)$$

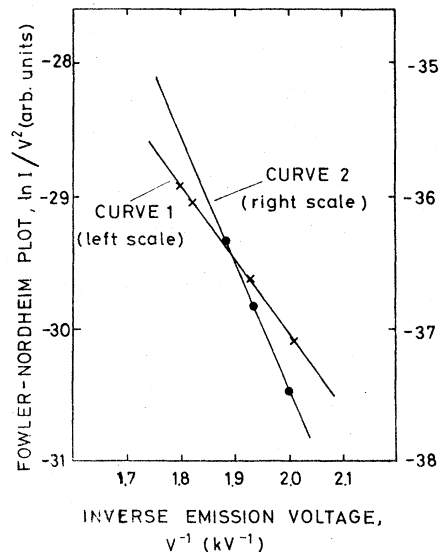


FIG. 14. Fowler-Nordheim plots of W-EuS emitter at a tip temperature of 10 K (curve 1) and 19 K (curve 2). The EuS-layer thickness was 580 Å before annealing, the tungsten tip radius was about 1000 Å.

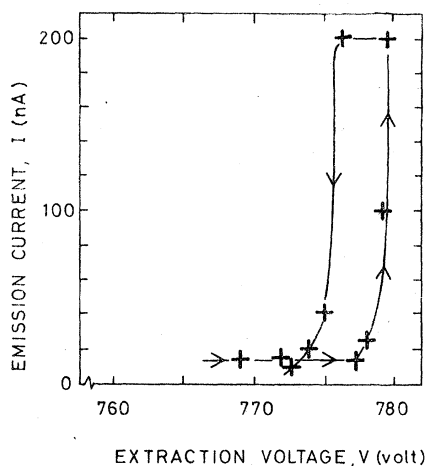


FIG. 15. Current-voltage characteristics for an emitter annealed above 1100 K, exhibiting a current-voltage hysteresis effect.

where ϕ_w is the average work function of the clean tungsten emitter. From FN plots for different tip temperatures and Eq. (14), a difference in barrier height of

$$\Delta\phi_i = \phi_i(T_c) - \phi_i(9K) = 0.12\text{eV}$$

was determined.¹⁹

For emitters annealed at high temperatures (>1100 K) the FN plots would be very nonlinear. Those emitters, which exhibit the steplike current-voltage characteristics shown in Fig. 12, also exhibit steplike current-voltage characteristics with an accompanying hysteresis effect as shown in Fig. 15. We assume that for these emitters a large number of impurity states has been introduced by the high annealing temperature. Presumably these impurities are S^{2-} vacancies due to preferential sulfur evaporation. At some electric field strength these vacancy states, which can bind two electrons, become field ionized and are left positively charged. The tunnel current into the EuS is then mainly determined by the positive space charge at the interface rather than by the applied external electric field. Thus a decrease in extraction voltage will not immediately cause a current reduction. Similar hysteresis effects have been observed by Ovshinsky,⁵⁰ Wachter,⁵¹ and Bayer.⁵²

D. Electron energy distribution, spin polarization, and field-emission pattern obtained with different annealing temperatures

1. Critical annealing at 840 K

The electron energy distributions which are typical for the various annealing temperatures are

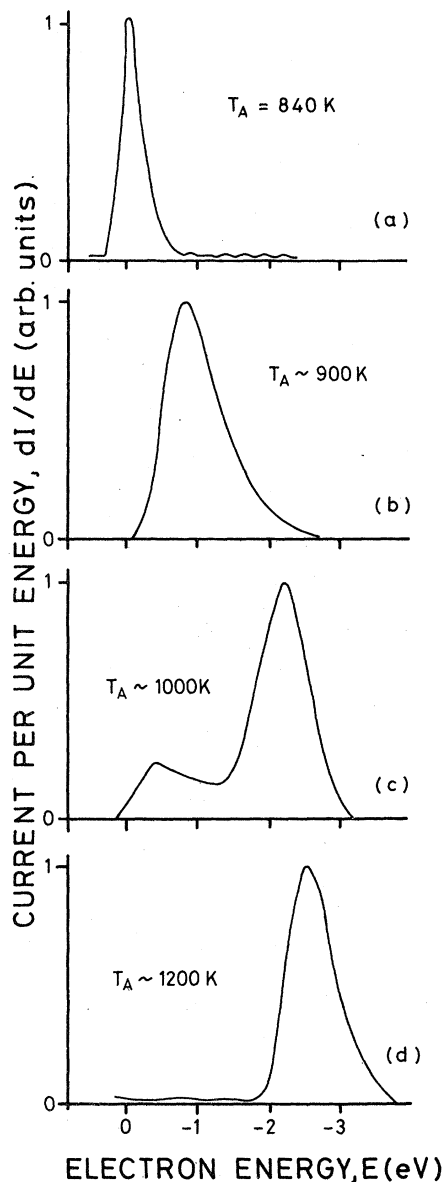


FIG. 16. Typical differential energy distributions for four different annealing temperatures. Going from (a) to (d) the Curie temperature increases from 16.6 K to above 22 K.

shown in Fig. 16. For T_A a most striking, very monoenergetic distribution is found which is shown in more detail in Fig. 17. In this case, the annealing time is also critical and was less than one second. The spin polarization associated with the monoenergetic beam is $85\% \pm 7\%$. The field-emission pattern does not show any symmetry. It consists of one or two bright spots, while the rest of the fluorescent screen is dark. Those emitters exhibit the strong temperature dependence of the electron current, which was shown in Fig. 10.

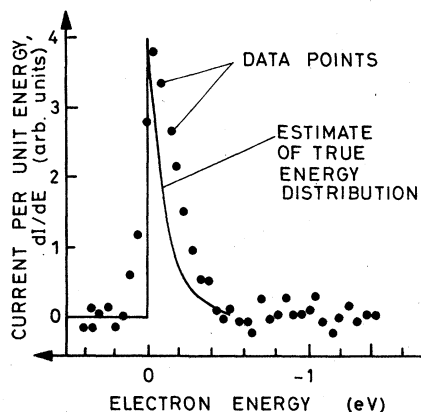


FIG. 17. Narrow energy distribution measured after critical annealing of the EuS layer at a temperature of 840 K. The energy resolution of the retarding-field analyzer was determined to be 150 meV. The distribution function given above as a solid curve has a width of 80 meV; this function folded with a Gaussian of 150-meV half-width gives a good approximation to the data points.

2. Annealing between 850 and 920 K

Now the field-emission pattern is symmetric and shows emission from the (112) planes of the tungsten emitter. A photograph, obtained with a $\langle 110 \rangle$ oriented tungsten tip, is given in Fig. 18. Sometimes the energy distribution exhibits only a single peak which is 0.5–1 eV below the Fermi level. Generally it displays the double-peak structure as shown in Fig. 16(c). The emission

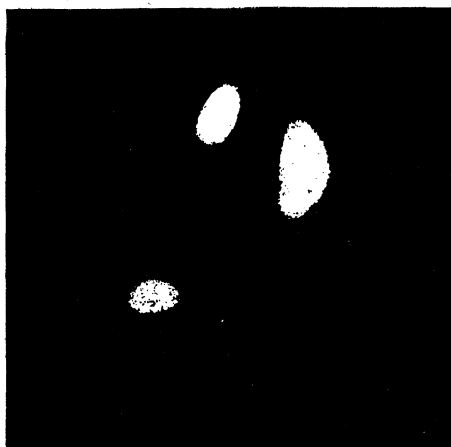


FIG. 18. Field-emission pattern obtained with an EuS-coated tungsten tip which had the $\langle 110 \rangle$ direction along the tip axis. In this sample only three of the normal four spots are observed; the emitting surfaces shown here are (211), $(2\bar{1}\bar{1})$, $(12\bar{1})$. The image is slightly distorted because of electron-optical aberrations. The full pattern consists of four spots which form a rectangle whose sides have a length ratio of 1:1.3.

current depends strongly upon temperature, and the polarization is high (85%). Apparently, the electrons suffer energy losses inside the EuS layer as indicated by the broadened and shifted energy distribution.

3. Annealing in the range 920–1080 K

After annealing at slightly higher temperature the emission pattern remains unchanged showing emission from the (112) planes of the clean tungsten emitter (cf. Fig. 18). The energy distribution is broader, and has a small peak at the tungsten Fermi level or slightly lower in energy, and a dominant peak several electronvolts lower in energy. The $I(T)$ and $P(T)$ curves are those shown in Fig. 10; the electron current still depends strongly upon tip temperature, and the polarization remains very high. The emission voltage for obtaining a given current is very low at 920 K. It increases with annealing temperature in the range 920–980 K.

We assume that the internal barrier is changed by a formation of a dipole layer at the W-EuS interface. Since the vacuum barrier does not limit the electron current, as has been inferred from the temperature dependence of the current, the field-emission pattern must be caused by barrier variations at the W-EuS interface. From the field-emission pattern it is concluded that the lowering of the internal barrier occurs only at the (112) planes of the tungsten emitter. This can be explained in the following way: From absorption studies of CsO on tungsten tips⁵³ combined with the assumption that the adsorption behavior of sulfur corresponds to that of oxygen (and Eu to Cs), it can be concluded that S atoms fit well into the surface voids of the (112) planes. Only in this very plane is the S density the same as the monolayer atom density of Eu which is adsorbed on the W planes. Therefore, at the (112) planes W-S-Eu complexes are formed with a higher density than anywhere else. They reduce the work function due to the positive charge of Eu ion. At all other crystal planes, excess W-S sites of opposite dipole moment can be accommodated.

E. Influence of electron traps

The large change in emission current with tip temperature and a value for the Curie temperature close to 17 K prove that the samples are crystallized. But the crystal structure must be disturbed due to the matching of the fcc EuS crystal to the tungsten (112) plane. A large number of defects can be expected to exist throughout the lattice. In addition, at these annealing temperatures sulfur is expected to evaporate preferentially from the

EuS layer leading to sulfur vacancies. These vacancies act as electron traps (similar to oxygen vacancies in EuO).⁵⁴ Due to repeated trapping on their way through the EuS layer, the electrons stay close to the bottom of the conduction band. The S^{2-} vacancy can bind two electrons with different binding energies; one represents a "shallow donor," the other is bound more tightly. Due to the applied electric field the "shallow donor" will be field ionized, that is, the loosely bound electron tunnels into the conduction band and an F^+ color center remains. A possible mechanism for the energy loss is thus capture by multiphonon or cascade processes, as discussed in detail by Stoneham.^{55,56}

The double-peak structure of the measured energy distributions is similar to the results of the theoretical considerations of Hrach⁵⁷ concerning Al-Al₂O₃-Au tunnel junctions. It follows from the trap model that the high-energy shoulder of the energy-loss peak must be exponential, which is indeed observed.²⁴ Two groups of electrons with significantly different energies are also predicted by Devreese.⁵⁸

The low-energy peak corresponds to an electron energy loss of ΔE (as compared with the energy of the Fermi level of tungsten). The measured values of ΔE were found to depend on film thickness d and extraction voltage V . The data agree with the formula

$$\Delta E = \phi_i - eF_e d / \epsilon, \quad (15)$$

where ϕ_i is the internal barrier height, ϵ is the static dielectric constant, $F_e = \alpha V / (R + d)$ is the external field strength, α is a factor dependent on the tip shape, and R is the tip radius. This can be understood from the emission model (cf. Fig. 11) because the energetic distance between the Fermi level and the bottom of the conduction band at the vacuum boundary increases with increasing film thickness and with increasing extraction voltage.

The electron spin polarization is high even when the energy distribution exhibits the double-peak structure. Because the high-energy peak contains only a small fraction of the total electron current, the low-energy electrons must be highly polarized. An energy-dependent polarization measurement as shown in Fig. 19 confirms this. The polarization of the high-energy electrons is zero within the experimental error, whereas the low-energy electrons ($E < -2$ eV) are highly polarized. Presumably the high-energy electrons are elastically scattered in the EuS layer and emitted into a wide solid angle (cf. Sec. IV F) and, therefore, it is conceivable that they experience depolarization due to spin rotation⁵⁹ in the external field of the

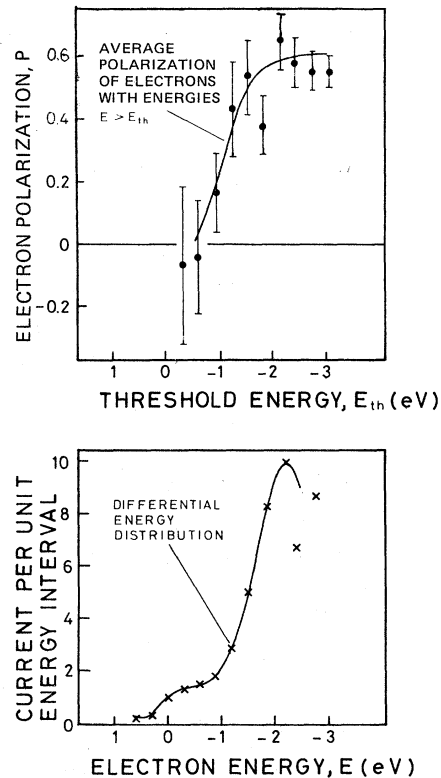


FIG. 19. Measurements on an emitter annealed at $T_A = 1050$ K with an EuS-layer thickness of 740 \AA . Upper diagram: electron polarization measurements as a function of the filter-lens threshold energy at $T = 11.5$ K. The measured polarization is the average for all electrons with energies $E > E_{th}$, where E is the emission energy with respect to the tungsten Fermi edge. Lower diagram: corresponding differential electron energy distribution.

tip region, but a total depolarization due to this effect is unlikely. Thus, we prefer a different explanation: The samples which were annealed at higher temperatures (like that of Fig. 19) do not exhibit the pronounced current-temperature dependence characteristic for the spin-filter action of the internal barrier. This suggests that all electrons entering the EuS layer through the W-EuS interface are unpolarized and that the low-energy electrons become polarized within the EuS layer while they are trapped. The here proposed ferromagnetic exchange interaction mediated by the trap is similar to that of the "bound magnetic polaron" discussed in the literature.^{54,60,61}

F. Anisotropy of EuS field emission

In measurements of the energy distribution on selected spots of the field-emission pattern, it was found that the shape of the energy distribution depended on which portion of the spot was ana-

lyzed. In the middle portion of the spot the intensity is high and the distribution contains a small "elastic" peak as well as a large inelastic peak. But near the edges the distribution contains only one peak.

This "anisotropy effect" is interpreted in the following way: the inelastic electrons are assumed to be emitted only in the normal direction because the electrons lose all their kinetic energy when they are trapped and leave the trap by tunneling in the direction of the electric field which is directed normal to the surface. Presumably, the "elastic electrons" are emitted into a wide solid angle because in the EuS lattice they undergo mainly scattering by phonons, processes in which very little kinetic energy is lost.

G. Magnetization and polarization of the EuS layer

The relative magnetization of EuS can be determined from the emission current [see Eq. (8)]. The direction of magnetization can be determined by polarization measurements. For a $\langle 111 \rangle$ -oriented tungsten tip three spots are observed forming a regular triangle at the $\langle 112 \rangle$ directions of tungsten. The direction of \vec{P} for these spots has been measured, and the results are shown in Fig. 20. The fact that the three spots differ in degree of polarization must be interpreted as due to different magnitudes of magnetization; but the fact that the three \vec{P} vectors of different length still add up to zero (within the accuracy of the measurement) is remarkable and not yet explained.

At low magnetic fields the direction of polarization lies tangential to the emitting surface, which leads to largely transversely polarized electrons.

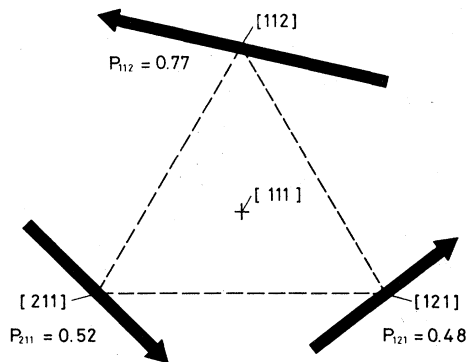


FIG. 20. Measured direction and magnitude of polarization of the electrons emitted from the $\langle 112 \rangle$, $\langle 121 \rangle$, and $\langle 211 \rangle$ surfaces of EuS-coated tungsten. In this experiment the tungsten tip had the $\langle 111 \rangle$ direction parallel to the tip axis. The polarization was found to be transverse. In this schematic drawing the tip is viewed head-on.

The direction of magnetization of EuS layer \vec{M} must be assumed antiparallel to \vec{P} , since the electron magnetic moment is antiparallel to the spin. This correlation of \vec{M} and \vec{P} was confirmed experimentally for the case of a high external magnetic fields.²²

H. Polarization in a high magnetic field, evidence for spin clusters

With a high field of 5 kG at the emitter, the magnetization determined from current measurements $M_I(T)$ shows a "high-temperature tail" which is absent in low magnetic field. As shown in Fig. 21 the $M_I(T)$ curve based on our current measurements agrees well with the curve $M_R(T)$ which is the magnetic red shift of (of the absorption edge in optical spectroscopy), according to Nolting's calculation.^{62,63} Both M_I and M_R are measures of the relative magnetization of the sample and also of the average $4f^7$ -electron polarization.

Noteworthy is the fact that the measured electron polarization $P(T)$ is significantly higher than M_I and M_R , especially at temperatures near and above the Curie point. A possible explanation for the high-field polarization above T_C can be given assuming the existence of spin clusters. Within a spin cluster, which might enclose 20–30 Eu^{2+} ions (inferred from the data in Fig. 21), the spins of the $4f^7$ electrons are ordered ferromagnetically among each other, giving the cluster a large total

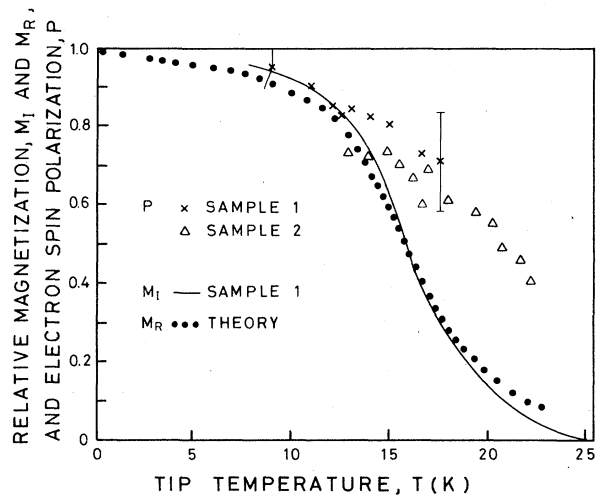


FIG. 21. Measurements with a high magnetic field of 5 kG at the emitter. The relative magnetization $M_I(T)$ as calculated from the measured emission current is compared with $M_R(T)$ from red-shift theory. Also shown is the measured spin polarization $P(T)$. The polarization in excess of the relative magnetization is taken as evidence for ferromagnetic spin clusters which order paramagnetically in the external magnetic field.

TABLE I. Performance parameters of low-energy polarized electron sources.

Source process utilized at	Low-energy Mott scattering Univ. Mainz, Stanford Univ., Univ. Münster (Ref. 20)	Fano effect of cesium Yale Univ. (Refs. (71, 72))	Optically pumped He discharge Rice Univ. (Refs. (73, 74))	Two-photon Ionization of Cs FOM Amsterdam (Refs. 75, 76)	Photoemission from GaAs ETH Zürich (Ref. 77)	Field emission from W-EuS Univ. Bielefeld (Ref. 23)
Polarization P	0.2	0.63	0.4	(goal 1.0)	0.4	0.85
Current I (A)	3.5×10^{-8}	2.5×10^{-8}	10^{-6}	(goal 10^{-7})	(goal 10^{-3})	10^{-8}
Emittance ϵ_0 (rad cm)	2×10^{-2}	2×10^{-2}	10^{-2}	10^{-1}	2×10^{-3}	8×10^{-7}
At energy E_0 (eV)	3×10^2	10^3	5×10^2	3×10^2	1	3
Energy width ΔE (eV)	0.6	3	0.5	0.5	0.2	0.1
$M_1 = IP^2$ (A)	1.4×10^{-9}	1.0×10^{-8}	1.6×10^{-7}	(10^{-7})	(1.6×10^{-4})	7.2×10^{-9}
$M_2 = M_1 / \epsilon_0^2 E_0$ (A/rad ² cm ² eV)	1.2×10^{-8}	2.5×10^{-8}	3.2×10^{-6}	(3×10^{-4})	(40)	3.8×10^5
$M_3 = M_2 / \Delta E$ (A/rad ² cm ² eV ²)	2×10^{-8}	8×10^{-9}	6×10^{-6}	(6×10^{-4})	(2×10^2)	4×10^4

spin.

Theoretically, such clusters were discussed by Kasuya and Yanase.⁶¹ Experimentally it was shown by Vitins and Wachter⁴⁵ that in antiferromagnetic EuTe very large spin clusters are built up around vacancies, the size of which depend upon the crystal temperature and the applied magnetic field. The clusters are formed by the overlap of the wave function of an impurity d electron with neighboring Eu ions, and the d - f exchange interactions couple the spins of the $4f$ electrons *ferromagnetically* to the spin of the d electron.

To explain the large electron polarization, we assume that most of the emission current comes from electrons which were temporarily trapped in vacancies. Around the vacancies spin clusters are built up and by spin exchange the trapped electrons obtain a polarization corresponding to the magnetization of a cluster. A spin cluster, ferromagnetically ordered, has a magnetization which is much higher than that of the sample, averaged over a large volume. If a magnetic field is applied the spin clusters will order paramagnetically with their spins aligned in field direction. Under the conditions stated in Fig. 21, the spin clusters will obtain a large paramagnetic order, explaining the measured electron polarization.

V. W-EuS EMITTER AS A SOURCE OF POLARIZED ELECTRONS

A W-EuS emitter, critically annealed, is an almost ideal polarized electron source for low-energy experiments. It is compared in its characteristics with other available sources in Table I. Only sources similar in design and intended for similar purposes can reasonably be compared by the common figure of merit which we call M_1 . Kessler²⁰ advocated the quantity M_2 (which he calls "beam quality"); we feel that that M_3 is the most useful figure for a critical evaluation of different sources. Not included in the table is the LEED source of polarized electrons⁶⁴⁻⁶⁷ for which the optimum performance characteristics are not yet known, but which could turn out to be an interesting source for low-energy experiments.

It would be unreasonable to extend this comparison to sources for high-energy accelerators. For example, the very successful polarized electron source of the Stanford Linear Accelerator Center (SLAC)^{68, 69} yields more current than a polarized proton target can stand. Therefore, a further current increase would be useless and, consequently, the factor I cannot be included in a figure of merit appropriate for such sources; the energy width is of no concern at SLAC as long as it lies below 1.5 kV; the emittance can be as large as the

injector acceptance.

For low-energy experiments the most useful sources are those which operate with a weak or without any magnetic field. If a strong magnetic field has to exist at the source and the beam has to be extracted from the field, an additional contribution to the beam emittance must be considered in order to take into account the unavoidable skewing of the electron trajectories in the magnetic fringe field.⁷⁰

The stability of the W-EuS source depends on the pressure in the emission chamber. At 5×10^{-10} Torr there is a noticeable decrease in current and degradation of the pattern after a time of about half an hour, probably caused by a contamination of the emitting surface with adsorbed gases. At pressures between 0.5 and 1×10^{-10} Torr no changes of the beam parameters are observed over times of several hours. The current of 10^{-8} A, given in Table I, is based on typical values with which our investigations were carried out. An upper limit for a polarized current, in particular for the monoenergetic and highly polarized beam, has not yet been determined.⁷⁸ Indications are that, with increasing extraction voltage, the emission intensities connected with the individual field-emission spots saturate at some level and therefore the electron beam current, obtained by selecting one of these spots, will saturate—most probably below 10^{-7} A.

VI. SUMMARY

By combining measurements of the field-emission current, spin polarization, electron energy distribution, and energy-selective spin polarization we have been able to develop a reasonable model for the emission process of electrons from W-EuS emitters. It has been shown that the W-EuS interface acts as a spin filter for electrons originating from the tungsten tip. The emission is governed by the internal barrier at the W-EuS interface. The external barrier is lowered due to the field penetration into the EuS layer; this barrier still prevents any emission from the $4f^7$

states, the highest occupied states in EuS.

It has been demonstrated that field emission studies together with polarization measurements can provide new information on the magnetic properties of the material deposited onto the tungsten tip. We can explain our experimental observations by assuming two ferromagnetic interactions: (i) indirect exchange via $5d$ states near the bottom of the conduction band which prevails in pure and slightly impure samples (S vacancies); and (ii) ferromagnetism mediated by the impurity states which dominates at high concentrations of S vacancies and is responsible for the formation of spin clusters. (An indirect superexchange via anion lattice could lead to antiferromagnetic ordering. This, however, can not be detected by means of polarization measurements.)

Energy distribution measurements yielded information on the composition of the crystal and the generation of S^{2-} vacancies with increasing annealing temperatures. Important for the field of polarized electron sources is the discovery of the critical annealing which leads to highly polarized ($P \sim 0.85$) and highly monoenergetic ($\delta E \sim 100$ meV) electrons. The field-emission source is distinguished by a very small emittance which means that the polarized beam can be decelerated without appreciable loss of intensity.

ACKNOWLEDGMENTS

In building the apparatus, preparing the Mott scattering foils, and producing the tungsten tips for the first measurements we had the valuable help of K. Schröder. For stimulating discussions, we thank N. Müller (Max-Planck-Institut, Garching bei München), W. Zinn (Institut für Festkörperphysik der Kernforschungsanlage Jülich), P. Wachter, and W. Nolting (Eidgenössischen Technischen Hochschule Zürich), and L. W. Swanson (Oregon Graduate Center). We gratefully acknowledge the cooperation of the technical staff of the Bielefeld Physics Department. This work was supported by the University of Bielefeld under Project No. 2854.

*Present address: Institut für Festkörperforschung, Kernforschungsanlage Jülich, 5170, Federal Republic of Germany.

†Present address: Physics Dept. Rice Univ., Houston, Tex. 77001.

‡Present address: Laboratorium für Festkörperphysik der Eidgenössischen Technischen Hochschule, CH-8093 Zürich, Switzerland.

¹C. Haas, *CRC Crit. Rev. Solid State Sci.* **1**, 47 (1970).

²P. Wachter, *CRC Crit. Rev. Solid State Sci.* **3**,

189 (1972).

³P. Wachter, in *Handbook on the Physics and Chemistry of Rare Earths*, edited by K. A. Gschneider, Jr. and L. Eyring (North-Holland, Amsterdam), Vol. 1 (to be published).

⁴T. R. McGuire and M. W. Shafer, *J. Appl. Phys.* **35**, 984 (1964).

⁵G. Busch, P. Junod, and P. Wachter, *Phys. Lett. A* **12**, 11 (1964).

⁶G. Busch and P. Wachter, *Phys. Kodens. Mater.* **5**, 232 (1966).

- ⁷L. Esaki, P. J. Stiles, and S. von Molnar, *Phys. Rev. Lett.* **19**, 852 (1967).
- ⁸E. Fues and H. Hellmann, *Z. Phys.* **31**, 465 (1930).
- ⁹G. Obermair, *Z. Phys.* **217**, 91 (1968).
- ¹⁰H. von Issendorff and R. Fleischmann, *Z. Phys.* **167**, 11 (1962).
- ¹¹W. T. Pimbley and E. W. Mueller, *J. Appl. Phys.* **33**, 238 (1962).
- ¹²M. Hofmann, G. Regenfus, O. Schärpf, and P. J. Kennedy, *Phys. Lett. A* **25**, 270 (1967).
- ¹³W. Gleich, G. Regenfus, and R. Sizmann, *Phys. Rev. Lett.* **27**, 1066 (1971).
- ¹⁴N. Müller, *Phys. Lett. A* **54**, 415 (1975).
- ¹⁵M. Campagna, T. Utsumi, and D. N. E. Buchanan, *J. Vac. Sci. Technol.* **13**, 193 (1976).
- ¹⁶Only recently, high polarizations were reported for field emission from metals (Ref. 17).
- ¹⁷G. Chrobok, M. Hofmann, G. Regenfus, and R. Sizmann, *Phys. Rev. B* **15**, 429 (1977).
- ¹⁸M. Müller, W. Eckstein, W. Heiland, and W. Zinn, *Phys. Rev. Lett.* **29**, 1651 (1972).
- ¹⁹E. Kisker, G. Baum, A. H. Mahan, W. Raith, and K. Schröder, *Phys. Rev. Lett.* **36**, 982 (1976).
- ²⁰J. Kessler, *Polarized Electrons* (Springer-Verlag, Berlin, 1976).
- ²¹M. S. Lubell in *Atomic Physics 5*, edited by R. Marrus, M. Prior, and H. Shugart, (Plenum, New York, 1977), pp. 325-373.
- ²²G. Baum, E. Kisker, A. H. Mahan, and K. Schröder, *J. Mag. Magn. Mater.* **3**, 4 (1976).
- ²³G. Baum, E. Kisker, A. H. Mahan, W. Raith, and B. Reihl, *Appl. Phys.* **14**, 149 (1977).
- ²⁴E. Kisker, A. H. Mahan, and B. Reihl, *Phys. Lett. A* **62**, 261 (1977).
- ²⁵D. A. Reed and W. R. Graham, *Rev. Sci. Instrum.* **43**, 1365 (1972).
- ²⁶Tungsten tips purchased from Field Electron and Ion Source Specialists Company, McMinnville, Ore. 97128.
- ²⁷Europium Sulfide was obtained from AERE (Harwell).
- ²⁸G. Sauerbrey, *Z. Phys.* **155**, 206 (1959).
- ²⁹Balzers Quartz Crystal Thin Film Monitor QSG 201.
- ³⁰S. Smoes, J. Drowart, and J. M. Welter, *J. Chem. Thermodynamics* **9**, 275 (1977).
- ³¹E. Kisker, *J. Phys. E* (to be published).
- ³²Electron detectors: ORTEC Model CA-017-100-300.
- ³³W. Legler, *Z. Phys.* **171**, 424 (1963).
- ³⁴W. Raith, in *Atomic Physics*, edited by B. Bederson, V. W. Cohen, and F. M. J. Pichanick, (Plenum, New York 1969), pp. 389-415.
- ³⁵Formvar, Type 7/95 S, provided by Monsanto Corp., Bircham Bend Plant, Springfield, Mass.
- ³⁶J. M. Pelmore, C. J. S. Chapman, J. M. Walls, G. G. Summers, and H. N. Southworth, *J. Phys. E* **9**, 96 (1976).
- ³⁷The carbon-resistance thermometers were furnished by Leybold Corp.
- ³⁸J. W. Gadzuk and E. W. Plummer, *Rev. Mod. Phys.* **45**, 487 (1973).
- ³⁹As shown by Gadzuk and Plummer (Ref. 38) about 99% of the transverse energy is converted into radial energy at a distance from the emitter of $10R$ (R is the radius) if no magnetic field is present. Since our magnetic field influences the electron path only over macroscopic dimensions this argument remains valid.
- ⁴⁰W. A. Thompson, F. Holtzberg, T. R. McGuire, and G. Petrich, in *AIP, Conf. Proc.* **5**, 827 (1971).
- ⁴¹It has been suggested by P. Wachter and by W. Zinn (private communications) that ϕ_i should vary as the spin-correlation function rather than as the magnetization. Both our $\ln I(T)$ data and the tunnel conductivity curves of Thompson *et al.* (Ref. 40), however, drop sharper at T_C than a spin-correlation function. Therefore, it was suggested by P. Wachter that the observed $I(T)$ dependence may be due to the combination of two effects: the change in carrier concentration by the change of ϕ_i and the change in electron mobility due to spin-disorder scattering near T_C .
- ⁴²W. Baltensperger, *J. Appl. Phys.* **41**, 1052 (1970).
- ⁴³G. Güntherodt, P. Wachter, and D. M. Imboden, *Phys. Kondens. Mater.* **12**, 292 (1971).
- ⁴⁴Recent theoretical work of W. Nolting (private communication) indicates that the usual assumption of a conduction band, split into two spin-polarized subbands, is only a limiting case where the coupling between the conduction electron and the core $4f^7$ electrons is very weak. In all other cases there is an overlapping of the pure spin states and mixed spin states.
- ⁴⁵J. Vitins and P. Wachter, *Phys. Rev. B* **12**, 3829 (1975).
- ⁴⁶R. Gomer, *Field Emission and Field Ionization* (Harvard University, Cambridge, Mass., 1961).
- ⁴⁷This approximate formula for the tip radius was obtained by calculating the field strength which reduces the external barrier by an amount equal to the W work function, which leads to $R(\text{Å}) = 0.7\alpha V_W$ (Volt), and then setting the form factor $\alpha = 1$ for simplicity (Ref. 48).
- ⁴⁸B. Reihl, Diplomarbeit (Universität Bielefeld, 1977).
- ⁴⁹G. Busch, M. Campagna, and H. C. Siegmann, *J. Appl. Phys.* **42**, 1781 (1971).
- ⁵⁰S. R. Ovshinsky, *Phys. Rev. Lett.* **21**, 1450 (1968).
- ⁵¹P. Wachter, *Phys. Lett. A* **41**, 391 (1972).
- ⁵²E. Bayer, *Physica Utr. B* **80**, 57 (1975).
- ⁵³L. W. Swanson and R. W. Strayer, *J. Chem. Phys.* **48**, 2421 (1968).
- ⁵⁴J. B. Torrance, M. W. Shafer, and T. R. McGuire, *Phys. Rev. Lett.* **29**, 1168 (1972).
- ⁵⁵A. M. Stoneham, in *Theory of Defects in Solids* edited by C. E. H. Bawn, H. Fröhlich, P. B. Hirsch and N. F. Mott (Clarendon, Oxford, 1975), pp. 522 ff.
- ⁵⁶A rough estimate shows that the latter process would have the cross section and transition probability necessary for creation of high-intensity energy-loss peak of Fig. 16 (c).
- ⁵⁷R. Hrach, *Czech. J. Phys. B* **18**, 1591 (1968).
- ⁵⁸If scattering on optical phonons is the dominant inelastic scattering mechanism, a "run-away" solution of the Boltzmann transport equation exists, which corresponds to electrons which travel through the layer without energy loss [J. R. Devreese, State University of Antwerp (private communication)].
- ⁵⁹W. Eckstein and N. Müller, *Appl. Phys.* **6**, 71 (1975).
- ⁶⁰Y. Shapira and T. B. Reed, *Phys. Rev. B* **5**, 4877 (1972).
- ⁶¹T. Kasuya and A. Yanase, *Rev. Mod. Phys.* **40**, 684 (1968).
- ⁶²W. Nolting, *Solid State Commun.* **21**, 1077 (1977).
- ⁶³In Ref. 62, only the curves for $B = 0$ and $B = 1 T$

- are given. We have interpolated between these curves to obtain the data for $B = 0.5$ T.
- ⁶⁴M. R. O'Neill, M. Kalisvaart, F. B. Dunning, and G. K. Walters, *Phys. Rev. Lett.* **34**, 1167 (1975); M. Kalisvaart, M. R. O'Neill, T. W. Riddle, F. B. Dunning, and G. K. Walters, *Phys. Rev. B* **17**, 1570 (1978).
- ⁶⁵R. Feder, N. Müller, and D. Wolf, *Z. Phys. B* **28**, 265 (1977).
- ⁶⁶R. L. Calvert, G. J. Russell, and D. Haneman, *Phys. Rev. Lett.* **39**, 1226 (1977).
- ⁶⁷T. W. Riddle, A. H. Mahan, F. B. Dunning and G. K. Walters, *J. Vacuum Sci. Technol.* (to be published).
- ⁶⁸M. J. Alguard, G. Baum, J. E. Clendenin, V. W. Hughes, M. S. Lubell, R. H. Miller, W. Raith, K. P. Schüler, and J. Sodja, *IEEE Trans. Nucl. Sci.* **NS-24**, 1603 (1977).
- ⁶⁹M. J. Alguard, R. D. Ehrlich, V. W. Hughes, J. Laidish, M. S. Lubell, W. Lysenko, K. P. Schüler, G. Baum, and W. Raith, in *Proceedings of the Ninth International Conference on High Energy Accelerators*, Stanford Linear Accelerator Center, May 1974 (U. S. Dept. of Commerce, Natl. Techn. Info. Serv., Springfield, Va., 1974), pp. 309-313.
- ⁷⁰W. Raith in *Physics of the One- and Two-Electron Atoms*, edited by F. Bopp and H. Kleinpoppen (North-Holland, Amsterdam, 1969), pp. 727-743.
- ⁷¹G. Baum, M. S. Lubell, and W. Raith, *Bull. Am. Phys. Soc.* **16**, 586 (1971).
- ⁷²P. F. Wainwright, M. J. Alguard, G. Baum, and M. S. Lubell, *Rev. Sci. Instrum.*, (to be published).
- ⁷³P. J. Keliher, R. E. Gleason, and G. K. Walters, *Phys. Rev. A* **11**, 1279 (1975).
- ⁷⁴G. K. Walters, Rice University (private communication).
- ⁷⁵E. H. A. Grannemann, M. Klewer, K. J. Nygaard, and M. J. Van der Wiel, *J. Phys. B* **9**, L87 (1976); E. H. A. Granneman, Thesis (University of Amsterdam, 1976) (unpublished).
- ⁷⁶For determining the emittance listed in this column we assumed that electrons of 0.03-eV energy are emitted from an area of 10^{-2} cm² in all directions.
- ⁷⁷D. T. Pierce, M. Meier, and P. Zürcher, *Appl. Phys. Lett.* **26**, 670 (1975); D. T. Pierce and F. Meier, *Phys. Rev. B* **13**, 5484 (1976).
- ⁷⁸For one tip, which had been prepared such that an electron beam with a broader energy distribution than 100 meV and a polarization of $P = 0.6$ was obtained, a stable current of 5×10^{-7} A was recorded.